PLANT SCIENCES

An MKP-MAPK protein phosphorylation cascade controls vascular immunity in plants

Hui Lin[1,2]†, Muyang Wang[2]†, Ying Chen[2], Kinya Nomura[3], Shugang Hui[4], Jinshan Gui[2], Xiawei Zhang[2], Yue Wu[2,5], Jiyun Liu[2], Qun Li[2], Yiwen Deng[2], Laigeng Li[2], Meng Yuan[4], Shiping Wang[4], Sheng Yang He[3,6], Zuhua He[1,2]*

Global crop production is greatly reduced by vascular diseases. These diseases include bacterial blight of rice and crucifer black rot caused by *Xanthomonas oryzae* pv. *oryzae* (*Xoo*) and *Xanthomonas campestris* pv. *campestris* (*Xcc*). The molecular mechanisms that activate vascular defense against such pathogens remains underexplored. Here, we show that an *Arabidopsis* MAPK phosphatase 1 (MKP1) mutant has increased host susceptibility to the adapted pathogen *Xcc* and is compromised in nonhost resistance to the rice pathogen *Xoo*. MKP1 regulates MAPK-mediated phosphorylation of the transcription factor MYB4 that negatively regulates vascular lignification through inhibiting lignin biosynthesis. Induction of lignin biosynthesis is, therefore, an important part of vascular-specific immunity. The role of MKP-MAPK-MYB signaling in lignin biosynthesis and vascular resistance to *Xoo* is conserved in rice, indicating that these factors form a tissue-specific defense regulatory network. Our study likely reveals a major vascular immune mechanism that underlies tissue-specific disease resistance against bacterial pathogens in plants.

INTRODUCTION

Plant vascular system that is crucial for plant growth and development (*1*). A number of pathogens invade the plant vascular system, causing severe disease symptoms and substantial reductions in crop yield. Vascular pathogens include *Xanthomonas oryzae* pv. *oryzae* (*Xoo*), which causes rice bacterial blight (*2*), *Xanthomonas campestris* pv. *campestris* (*Xcc*) that underlies crucifer black rot, *Ralstonia solanacearum*, which results in bacterial wilt, and *Verticillium dahliae* responsible for cotton wilt. These pathogens can infect plants through wounds, leaf hydathode water pores, or roots (*3*), as observed for *Xoo* (*2*), *Xcc* (*4*), *R. solanacearum* (*5, 6*), and *V. dahlia* (*7, 8*). They then multiply in and block xylem vessels, resulting in systemic spread, tissue damage, and plant death (*2, 9*). However, current understanding of plant-pathogen interactions relies mainly on pathogens that infect leaf mesophyll tissues or broad-spectrum disease resistance to multiple pathogens with different lifestyles [as exampled in (*10–12*)]. Despite the agricultural impact of vascular pathogens, little is understood about the biochemical and molecular mechanisms underlying plant vascular immunity. Compared to other immune responses (*13–15*), our knowledge of plant defenses that target pathogens in the vasculature remains limited (*16*).

Coevolution of plants and vascular pathogens has likely shaped plant vascular immunity so that this defense system has both common and unique features compared to mesophyll pathogen defense (*16*). Tissue-specific infection has been reported for *Xanthomonadaceae* (*17*). For example, vascular xanthomonads colonize water-transporting xylem and extend along with the vascular system, while nonvascular *Xanthomonas* invade the mesophyll and cause localized symptoms (*18, 19*). The genomes of *Xoo* and *Xoc* (*X. oryzae* pv. *oryzicola*), two representative xylem and mesophyll xanthomonads, encode secreted transcription activator–like effectors (*20, 21*). These effectors can activate either host susceptibility (*S*) genes, leading to virulence, or resistance (*R*) genes resulting in tissue-specific resistance. It has been reported that vascular *Xanthomonas* pathogens secrete cell wall–degrading enzymes during infection, such as cellulases (clsA and cbsA), xylanase (xyn), pectinase (pglA), and esterase (lipA) (*22–24*). These enzymes also induce host immune responses. cbsA, a cellobiohydrolase that degrades cell walls, was found to be enriched in vascular *Xanthomonas* subgroups and lost in nonvascular *Xanthomonas* species (*25*). The evolution of this enzyme may have promoted a switch from nonvascular to vascular colonization, suggesting that a single locus can shift tissue-specific infection in closely related pathogens (*25, 26*). This divergence of pathogen lifestyles may have shaped tissue-specific plant immune responses. This raises a fundamental question: How do different resistance genes activate tissue-specific immune responses upon detecting pathogens with different lifestyles?

As one of the most abundant cell wall components and an important secondary metabolite in plant growth and development, lignin has been implicated in effective defense responses in plants. Lignin builds a physical barrier that blocks vessels or fills extracellular spaces, thus impeding bacterial multiplication and movement and acting as a key factor in vascular defense (*27–29*). *Arabidopsis*, soybean, and rice genes linked to lignin biosynthesis were up-regulated during pathogen infection, resulting in increased lignin levels and reinforcing the cell wall–based defense (*27–29*). Consistently, many lignin biosynthesis genes are highly expressed in plant vascular bundles (*30*). Moreover, previous studies have shown that several MYB family transcription factors regulate expression of lignin biosynthesis genes (*30–32*). Notably, MYB4 represses lignin biosynthesis, as seen in studies examining the plant response to ultraviolet light (*33–35*). However, the molecular links between the plant immune machinery and lignin-based vascular defense remain largely unexplored.

[1]School of Life Science and Technology, ShanghaiTech University, Shanghai 201210, China. [2]National Key Laboratory of Plant Molecular Genetics, CAS Centre for Excellence in Molecular Plant Sciences, Shanghai Institute of Plant Physiology and Ecology, Chinese Academy of Sciences, Shanghai 200032, China. [3]Department of Biology, Duke University, Durham, NC, USA. [4]National Key Laboratory of Crop Genetic Improvement, National Center of Plant Gene Research (Wuhan), Huazhong Agricultural University, Wuhan 430070, China. [5]University of the Chinese Academy of Sciences, Beijing 100049, China. [6]Howard Hughes Medical Institute, Duke University, Durham, NC, USA.
*Corresponding author. Email: zhhe@cemps.ac.cn
†These authors contributed equally to this work.

The vascular pathogens *Xoo* and *Xcc* and the leaf mesophyll cell pathogen *Xoc* serve as comparative models for investigating vascular-specific resistance. Here, we report that mitogen-activated protein kinase (MAPK) phosphatase 1 (MKP1) and its target kinases MPK3 and MPK6 form a signaling cascade that promotes vascular defense in both *Arabidopsis* and rice. We found that nonhost resistance (NHR) to *Xoo* is lost in *Arabidopsis mkp1* mutant, leading to *Xoo* growth in the leaf veins. The corresponding rice *Osmkp1* mutant exhibited enhanced host susceptibility to *Xoo*. Pathogen infection attenuates the MAPK phosphorylation pathway by inducing the *MPK1* gene, leading to inactivation of the MYB transcription factors that negatively regulate lignin biosynthesis genes. This regulatory cascade enhances lignin production and, thus, disease resistance against vascular pathogens. Our study uncovers a previously unappreciated molecular mechanism that contributes to plant vascular defense that is conserved in different plant species.

RESULTS

MKP1 controls vascular defense in *Arabidopsis*

To uncover the mechanism(s) that regulate plant vascular defense, we screened an ethylmethane sulfonate–mutagenized *Arabidopsis* Col-0 population challenged with *Xoo*, which does not usually infect *Arabidopsis*. The *ntx1* (nonhost disease resistance to *Xoo* 1) mutant developed disease symptoms indicating loss of NHR to the *Xoo* strain PXO99A (Fig. 1A). To examine *Xoo* growth in *ntx1* leaves, we created a beta-glucuronidase (GUS)–expressing *Xoo* strain. Notably, PXO99A-*GUS* colonized and proliferated in *ntx1* leaf veins (Fig. 1A), suggesting that vascular defense against *Xoo* is defective in *ntx1*. In addition to compromised NHR to the nonadapted pathogen *Xoo*, the *ntx1* mutant was more susceptible to the adapted vascular pathogen *Xcc* (Fig. 1B).

We next determined whether the loss of vascular resistance in the *ntx1* mutant is specific to vascular pathogens rather than loss of common NHR or basal defense. *Xanthomonas citri* subsp. *citri* (*Xac*) and *Xanthomonas campestris* pv. *vesicatoria* (*Xcv*) caused citrus bacterial canker and pepper bacterial spot disease, respectively (*36–40*), the destructive diseases of citrus and pepper. We found that *ntx1* was not more susceptible than wild-type Col-0 to nonhost and nonvascular *Xoc*, *Xac*, and *Xcv* (fig. S1, A to C). Last, we found that *ntx1* plants showed enhanced basal resistance to a leaf mesophyll–specific bacterial pathogen *Pseudomonas syringae* pv. *tomato* (*Pst* DC3000) (fig. S2A), with marked increases in transcript abundance of the salicylic acid (SA) pathway genes *ICS1* and *PR1* (fig. S2, B and C). These results strongly suggest that *NTX1* is specifically involved in vascular resistance rather than a more general process.

We cloned the *NTX1* gene using polymerase chain reaction (PCR)–based genetic mapping coupled with genome sequencing (fig. S3A). We found that the *ntx1* allele carries a G-to-A transition at nucleotide position 1416 in the *MKP1* (*At3G55270*) gene, which encodes MKP1. This G-A transition causes an Arg^{241}-Gln (MKP1^{R241Q}) missense mutation in the dual-specificity phosphatase catalytic site domain (fig. S3B). Consistent with the known functions of MKP1 in plant development (*41*), the *ntx1* plants displayed developmental defects, including decreased biomass, reduced seed setting due to abortive stamens, and larger seeds compared to the wild-type plants (fig. S3C).

To confirm the molecular identity of *NTX1*, we generated a *pMKP1::MKP1* complementation transgene and transformed it into the *ntx1* mutant. The *pMKP1::MKP1* transgene fully restored vascular resistance to *Xoo*. We also used CRISPR-Cas9 to generate a *MKP1* knockout line (*CR-mkp1*) in the Col-0 background and found that *CR-mkp1* plants phenocopied the *ntx1* mutant, displaying a loss of resistance to *Xoo* (Fig. 1C and fig. S3D). Together, these results link MKP1 function to vascular resistance against *Xoo* in *Arabidopsis*.

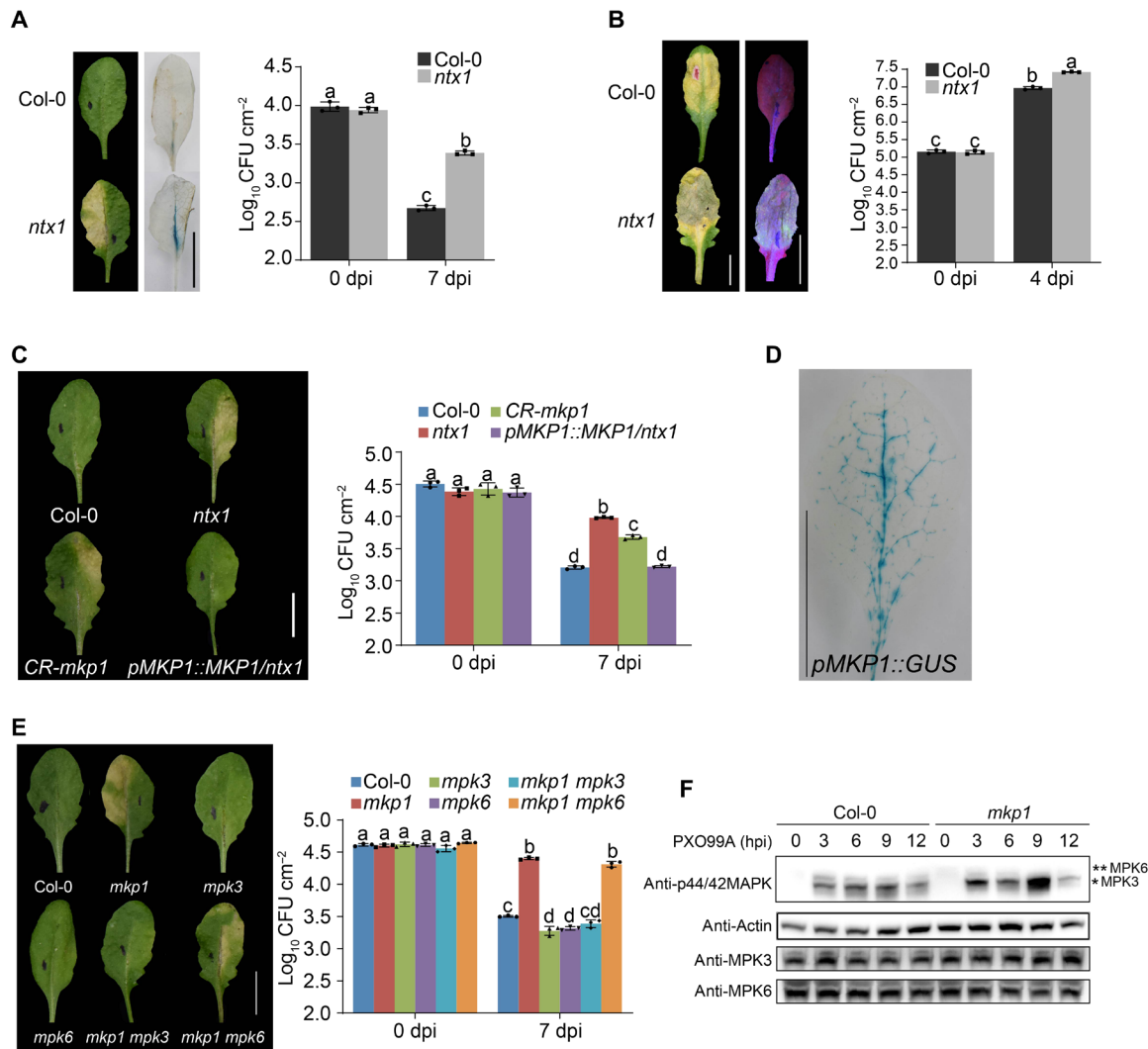### MKP1 regulates vascular resistance to *Xoo* by inactivating MPK3

We examined the expression of *MKP1* during *Xoo* infection and found that *MKP1* expression was induced by *Xoo* (fig. S4A). We also generated *pMKP1::GUS* fusion reporter plants and performed GUS histological analysis. Strong GUS activity was observed in vascular bundles (Fig. 1D), consistent with the idea that MKP1 functions in the vascular defense. We also carefully examined the potential cellular changes in *mkp1* using transmission electron microscopy (TEM) and found that vascular bundles were smaller in leaf sections of *mkp1* compared to wild-type plants, with no obvious change in cell wall thickness (fig. S4, B and C). These changes may explain the weak growth phenotype of *mkp1*.

On the basis of its predicted biochemical function, we hypothesized that MKP1 might regulate vascular defense by controlling MAPK activity, which plays a known role in plant immunity (*42*). Because MKP1 was previously shown to specially deactivate MPK3 and MPK6 via dephosphorylation (*43*), we analyzed the interaction of MKP1 with MPK3 and MPK6 using both the yeast two-hybrid (Y2H) and split luciferase complementation (SLC) assays. MKP1 interacted with MPK3 and MPK6 in both assays (fig. S5, A and B). Furthermore, we confirmed that MPK3 and MPK6 were dephosphorylated in vitro by MKP1 but not the catalytically inactive mutant variant MKP1^{R24IQ} [R^{241} is the conserved residue of the signature catalytic motif C(X)$_5$R of the tyrosine/dual-specificity protein phosphatases] (fig. S5, C and D).

We generated *mkp1 mpk3* and *mkp1 mpk6* double mutants by crossing *mkp1* with the single mutants *mpk3* and *mpk6*. When inoculated with *Xoo*, the *mkp1 mpk6* double mutant displayed *mkp1*-like susceptibility to *Xoo*, whereas the *mkp1 mpk3* double mutant exhibited Col-0–like resistance to *Xoo* (Fig. 1E). These results suggest that MKP1 regulates vascular resistance to *Xoo* through MPK3, rather than MPK6 inactivation, to regulate the vascular resistance against *Xoo*. To test this hypothesis, we analyzed phosphorylation of MPK3 and MPK6 during *Xoo* infection and found that *Xoo* inoculation strongly induced MPK3 phosphorylation but only slightly induced MPK6 phosphorylation (Fig. 1F). Furthermore, MPK3 phosphorylation was increased in the *mkp1* mutant, in contrast to MPK6 (Fig. 1G). These results suggest that MKP1-mediated dephosphorylation and inactivation of MPK3 underlies vascular resistance against *Xoo*.

Lignin plays a critical role in vascular resistance to *Xoo*

Given that *mkp1* plants showed enhanced resistance to *Pst* DC3000 (fig. S2A), with marked increases in the transcript abundance of SA pathway genes *ICS1* and *PR1* (fig. S2, B and C), and that SA and ROS (reactive oxygen species) play important roles in disease resistance (*44, 45*), we measured the SA and ROS levels during *Xoo* infection. We found that SA and ROS accumulation were not significantly induced by *Xoo* in *mkp1* plants compared to wild-type Col-0 plants (fig. S6, A to C), suggesting that the vascular defense mediated by MKP1 does not involve SA and ROS. Next, we performed an RNA transcriptome analysis of wild-type Col-0 and *mkp1* mutant plants infected with PXO99A. We found that genes linked to a range of

Fig. 1. *MKP1* mutants have reduced vascular resistance to *Xoo* and *Xcc*. (**A**) *PXO99A-GUS* populates the leaf veins of *ntx1* plants. Disease symptoms, GUS staining, and *Xoo* levels were measured in wild-type Col-0 and *ntx1/mkp1* mutant plants 7 days after infiltration with *Xoo* strain PXO99A and GUS-labeled *PXO99A-GUS* [2×10^7 colony-forming unit (CFU) ml^{-1}]. (**B**) Disease symptoms, green fluorescent protein (GFP) fluorescence, and growth of *Xcc* in Col-0 and *ntx1* at 4 dpi with GFP-labeled *Xcc*8004-*GFP* (1×10^7 CFU ml^{-1}). (**C**) Genetic complementation of *MKP1* in *ntx1* plants. Disease symptoms and bacterial populations were recorded at 7 days post inoculation (dpi) with PXO99A in Col-0, *ntx1*, *CR-mkp1*, and *pMKP1::MKP1/ntx1*. (**D**) GUS staining of *pMKP1::GUS* transgenic plants demonstrated that *MKP1* was mainly expressed in the vascular bundles. Scale bar, 1 cm. (**E**) The nonhost *Xoo* susceptibility phenotype of *mkp1* was restored by a mutation in MPK3 but not MPK6, showing that the double-mutant *mkp1 mpk3* restored the wild-type NHR to *Xoo*, 7 dpi with PXO99A. Data were shown as means ± SD ($n = 3$). Letters indicate significant differences ($P < 0.05$) determined by two-way analysis of variance (ANOVA) with Tukey's test. Scale bar, 1 cm. Experiments were repeated three times with similar results. (**F**) Kinase activation of MPK3 but not MPK6 was induced by *Xoo* inoculation. Proteins were prepared from leaf samples for in-gel kinase assay at the indicated times. hpi, hours post inoculation.

biological processes showed differential expression in *mkp1* compared to the wild-type plants (fig. S7A). Almost all genes of the lignin biosynthesis pathway, including *PAL1*, *C4H*, *4CL1*, and *COMT1*, were down-regulated in *mkp1* during *Xoo* infection (Fig. 2A and fig. S7B). Thus, we hypothesized that reduced lignin biosynthesis might contribute to the compromised vascular defense in the *mkp1* mutant. We found that, although lignin was induced by PXO99A in both the wild type and *mkp1*, the degree of lignin accumulation was markedly reduced in *mkp1* plants (Fig. 2B). Cell wall autofluorescence and phloroglucinol staining confirmed decreased lignin accumulation in the xylems of *mkp1* leaf veins (Fig. 2C and fig. S7C).

MPK3-mediated phosphorylation of MYB4 negatively regulates lignin biosynthesis

The transcriptional repressor MYB4 has previously been shown to negatively regulate expression of lignin biosynthesis genes and is specifically expressed in leaf veins (fig. S7D) (*30*). We therefore hypothesized that MPK3 phosphorylates and activates MYB4 and that the levels of active MPK3 and MYB4 might therefore be higher in *mkp1* plants than in wild-type plants. To test this hypothesis, we performed several protein-protein interaction assays, including Y2H, SLC, and in vitro pull-down, and found that MPK3-MYB4 interact (Fig. 2D and fig. S7, E and F). Coimmunoprecipitation (coIP) confirmed that MPK3 and MYB4 interact in planta (Fig. 2E).

Fig. 2. MPK3 phosphorylates MYB4 to regulate lignin biosynthesis. (**A**) Differential expression of lignin biosynthetic genes induced by *Xoo* in wild-type Col-0 and *mkp1* as revealed by RNA sequencing (RNA-seq). Many lignin biosynthesis genes were less induced in *mkp1* as compared with Col-0. FPKM, Fragments per kilobase of exon per million reads mapped. (**B**) Lignin quantification in leaves at 12 hours infiltrated with *Xoo* and *Xcc*. Data were shown as means ± SD ($n = 3$). Asterisks represented statistical significance (***$P < 0.001$, Student's *t* test). ns, not significant. Experiments were repeated three times. (**C**) Cell wall autofluorescence and relative fluorescence intensity of Col-0 and *mkp1* infiltrated with *Xoo*. Note that less lignification of the leaf vessel was induced by *Xoo* in *mkp1* as compared with Col-0. Scale bar, 50 μm. Data were shown as means ± SD ($n = 10$). Letters indicated significant differences ($P < 0.05$) determined by two-way ANOVA with Tukey's test. Experiments were repeated three times. (**D** and **E**) MPK3 interacts with MYB4, as revealed by Y2H screen (D) and coimmunoprecipitation (coIP) assay (E). SD/-Trp-Leu-His, synthetic dropout (SD) media lacking leucine, tryptophan, and histidine; SD/-Leu -Trp, SD media lacking leucine and tryptophan; 3AT, 3-aminotriazole. MPK3-GFP and MYB4-MYC in transgenic *Arabidopsis* plants were purified and immunodetected using anti-GFP or anti-MYC antibody. (**F**) MPK3 phosphorylates MYB4 in vitro. MPK3-MBP (myelin basic protein), MYB4-His, MKK4^{DD}-MBP (T224D/S230D), and MKK5^{DD}-MBP (T215D/S221D) were expressed in *E. coli* and purified for in vitro phosphorylation assays. MYB4-His was incubated at 30°C for 1 hour then separated on a Phos-tag gel. CBB, Coomassie brilliant blue staining for loading control.

Next, we tested whether MPK3 can phosphorylate MYB4 in vitro. The constitutively active MKK4^{DD} (T224D/S230D)/MKK5^{DD} (T215D/S221D) mutant strongly activates endogenous MPK3 and MPK6 (46). Coincubation of recombinant MYB4-His with MPK3–myelin basic protein (MBP) in the presence or absence of MKK4^{DD}/MKK5^{DD} resulted in a slow migrating MYB4-His band on Phos-tag SDS–polyacrylamide gel electrophoresis, indicating that MPK3 can phosphorylate MYB4-His (Fig. 2F).
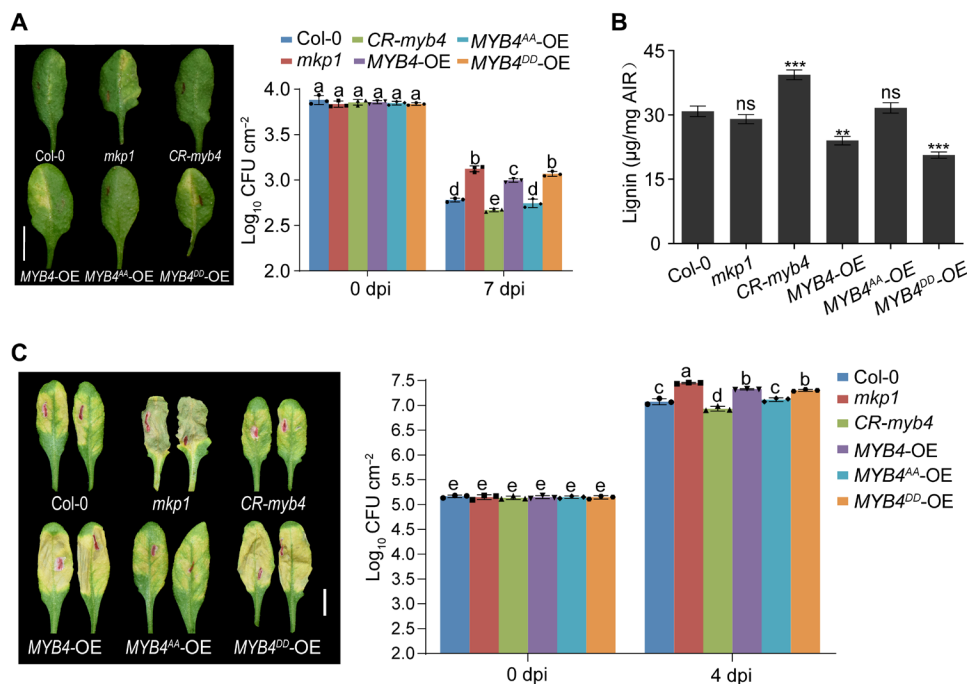
Phosphorylation of MYB4 suppresses vascular defense by inhibiting lignin biosynthesis

We previously predicted that MPK3 might phosphorylate MYB4 at two sites, Ser^4 and Thr^{221} (47). Thus, we generated loss-of-phosphorylation (MYB4^{AA}, Ser^4/Thr^{221} mutated to Ala) and phosphomimetic (MYB4^{DD}, Ser^4/Thr^{221} mutated to Asp) mutant variants of MYB4. Both MYB4^{AA} and MYB4^{DD} could still interact with MPK3 (fig. S7G). We used CRISPR-Cas9 editing to generate an MYB4 knockout line, CR-myb4, and created transgenic lines overexpressing MYB4-Myc (MYB4-OE), MYB4^{AA}-Myc (MYB4^{AA}-OE), or MYB4^{DD}-Myc (MYB4^{DD}-OE) (fig. S8, A and B). Similar to the mkp1 mutant, NHR was compromised in both MYB4-OE and MYB4^{DD}-OE transgenic plants in response to Xoo inoculation (Fig. 3A). We observed that the phosphorylated/active form MYB4^{DD} was more stable than the nonphosphorylated/inactive form MYB4^{AA} (fig. S8C). This was confirmed by following protein degradation (fig. S8D), suggesting that MYB4 might be subjected to dynamic control by protein phosphorylation and degradation.

MYB4 is known to bind the promoter of C4H, thus repressing expression of critical rate-limiting regulator of lignin biosynthesis (33, 34). We found that C4H was up-regulated in CR-myb4 and down-regulated in MYB4-OE and MYB4^{DD}-OE transgenic lines as compared with wild-type plants (fig. S8E). CR-myb4 lines consistently accumulated more lignin, whereas MYB4-OE and MYB4^{DD}-OE transgenic lines accumulated less lignin than wild type (Fig. 3B). Collectively, these data indicate that the phosphorylation-mediated activation of MYB4 by MPK3 suppress lignin biosynthesis, thus compromising vascular resistance to Xoo in mkp1 plants. Similar results were also observed with Xcc inoculation (Fig. 3C). These data together strongly suggest that MYB4 negatively regulates resistance to both adapted and nonadapted vascular pathogens through inhibiting lignin biosynthesis.

OsMKP1 regulates vascular resistance in rice

The rice genome encodes an MKP1 homolog, OsMKP1 (fig. S9A) (48). To investigate whether OsMKP1 is also involved in rice vascular defense against Xoo, we generated CRISPR-Cas9 knockout mutant (CR-Osmkp1) and OsMKP1 overexpression (OsMKP1-OE) lines (fig. S9B). Xoo proliferates and spreads within the xylem (fig. S9C). As in Arabidopsis, OsMKP1 expression was induced by Xoo (fig. S9D). Furthermore, CR-Osmkp1 plants exhibited enhanced susceptibility to Xoo in comparison with wild-type Nipponbare (NIP) plants. CR-Osmkp1 plants had also decreased lignin accumulation and decreased PR gene expression during Xoo infection (Fig. 4, A to C, and fig. S9, E and F). In contrast, OsMKP1-OE exhibited enhanced resistance

Fig. 3. Phosphorylation of MYB4 suppresses vascular defense by inhibiting lignin biosynthesis. (**A**) Disease symptoms (left) and bacterial growth (right) in Col-0, mkp1, CR-myb4, MYB4-OE, MYB4^{AA}-OE, and MYB4^{DD}-OE at 7 dpi with PXO99A. The wild-type MYB4 and the site mutation variants (MYB4^{DD} and MYB4^{AA}) were ectopically expressed (OE) as a MYC fusion protein. Scale bar, 1 cm. (**B**) Leaf lignin quantification indicated that lignin biosynthesis was inhibited by overexpression of MYB4 and MYB4^{DD} but not MYB4^{AA}. (**C**) MYB4 also negatively regulates resistance to Xcc. Disease symptoms (left) and bacterial growth (right) of Xcc in Col-0, mkp1, CR-myb4, MYB4-OE, MYB4^{AA}-OE, and MYB4^{DD}-OE at 4 dpi with Xcc8004. Scale bar, 1 cm. Data were shown as means ± SD (n = 3). Asterisks represented statistical significance (**P < 0.01 and ***P < 0.001, Student's t test) (B). Letters indicated significant differences (P < 0.05) determined by two-way ANOVA with Tukey's test (A to C). Experiments were repeated three times.

to *Xoo* (Fig. 4, A to C), although lignin accumulation was only slightly increased (fig. S9E).

Xoo invades systemically through the xylem tissue, while *Xoc* is a nonvascular pathogen and colonizes the intercellular spaces of mesophyll parenchyma. To determine whether MKP1-mediated resistance is also specific to vascular pathogens in rice, we inoculated the rice plants with *Xoc*. *CR-Osmkp1* plants showed enhanced resistance, whereas *OsMKP1*-OE plants displayed decreased resistance to *Xoc*, compared with wild-type NIP plants (Fig. 4D). In addition, similar to *Arabidopsis*, *CR-Osmkp1* was more susceptible to the nonadapted vascular pathogen *Xcc*8004 (Fig. 4E). Therefore, OsMKP1 plays a conserved role in the vascular defense in the dicot *Arabidopsis* and the monocot rice.
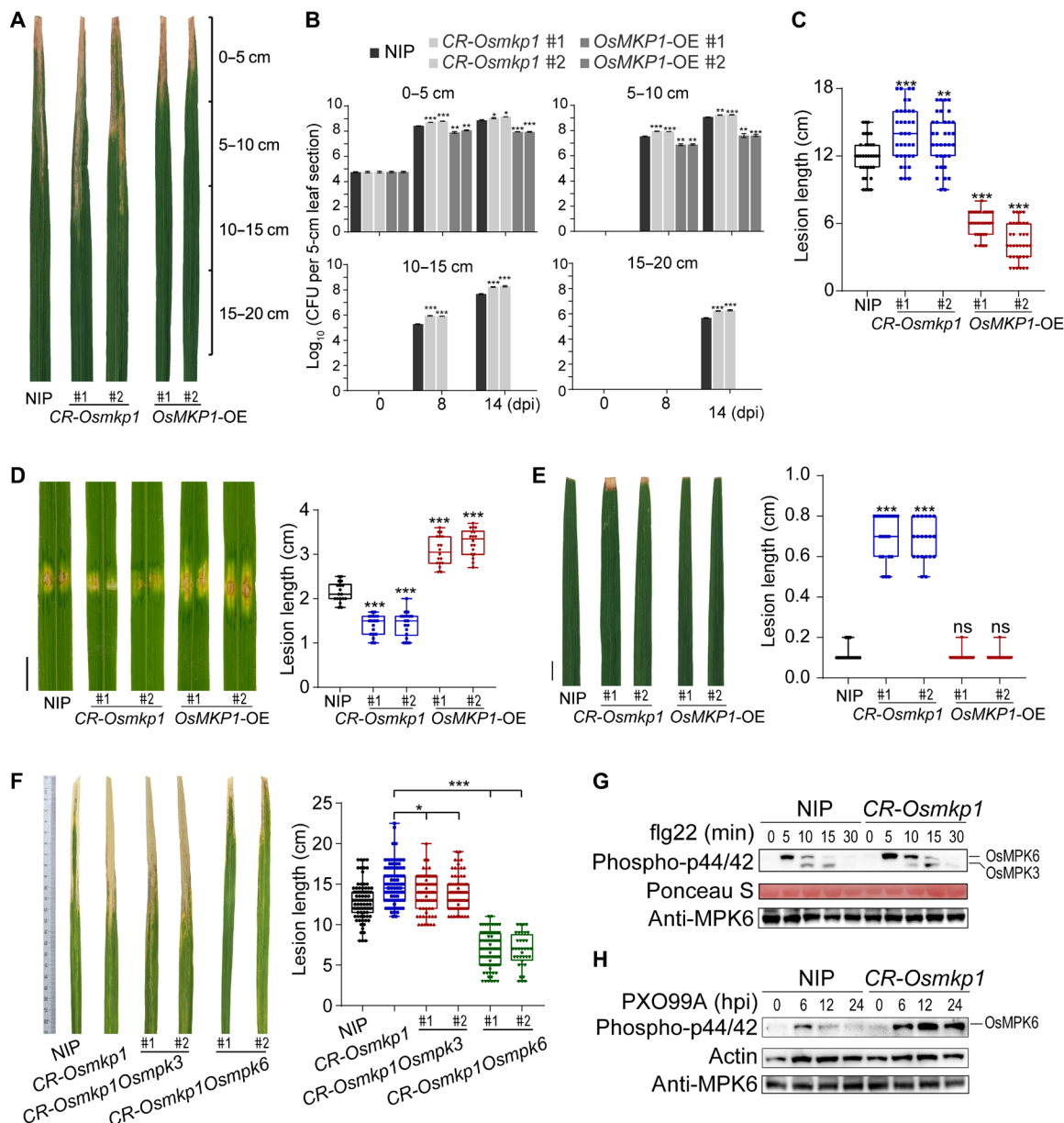
Fig. 4. OsMKP1 mediates *Xoo* resistance through OsMPK6 dephosphorylation. (**A** and **B**) Population size and distribution of *Xoo* in leaves of 2-month-old wild-type NIP, *CR-Osmkp1*, and *OsMKP1*-OE following clip inoculation. Bacterial populations in 5-cm leaf segments were measured at 0, 8, and 14 dpi. (**C**) Lesion lengths of NIP, *CR-Osmkp1*, and *OsMKP1*-OE inoculated with PXO99A [optical density at 600 nm (OD$_{600}$), 1.0] at 14 dpi. (**D**) Lesions (left) and statistical analysis (right) of NIP, *CR-Osmkp1*, and *OsMKP1*-OE inoculated with *Xoc* strains RS85. OsMKP1 negatively regulated resistance to *Xoc*. Scale bar, 1 cm. (**E**) Lesions and statistical analysis of NIP, *CR-Osmkp1*, and *OsMKP1*-OE inoculated with *Xcc*8004. (**F**) Disease symptoms of representative leaves (left) and lesion lengths (right) of NIP, *CR-Osmkp1*, *CR-Osmkp1Osmpk3*, and *CR-Osmkp1Osmpk6* inoculated with PXO99A at 14 dpi. Data were shown as means ± SD; $n > 20$ (C to F) and $n = 3$ (B). Asterisks represented statistical significance (*$P < 0.05$, **$P < 0.01$, and ***$P < 0.001$, Student's *t* test) (B to F). Experiments were repeated three times with similar results. (**G**) OsMPK3 and OsMPK6 activation by flg22 treatment. Two-week-old seedlings of NIP and *CR-Osmkp1* were treated with flg22 (1 μM) for the indicated times for protein preparation. The phosphorylated OsMPK3 and OsMPK6 were detected using the anti-p44/42 MPK antibody, with Ponceau S staining as loading control. (**H**) MPK6 was stronger activated in *CR-Osmkp1* infected by PXO99A as compared with NIP.

Next, we investigated the role of OsMKP3 and OsMPK6 in rice vascular defense. Both factors interact with OsMKP1 (fig. S10, A and B). We used CRISPR-Cas9–based editing to create *CR-Osmkp1Osmpk3* and *CR-Osmkp1Osmpk6* double knockout mutants (fig. S10C). *CR-Osmkp1Osmpk6* plants showed significantly enhanced resistance to *Xoo*, whereas *CR-Osmkp1Osmpk3* had only slightly increased disease resistance in comparison with the *CR-Osmkp1* single mutant (Fig. 4F). These data suggest that rice OsMPK3 and OsMPK6 both negatively regulate disease resistance to *Xoo*, with OsMPK6 playing a more prominent role in regulation. Consistently, an immunoblot analysis of flg22/PXO99A-induced phosphorylation of OsMPK3 and OsMPK6 revealed that OsMPK6 exhibited a greater increase in phosphorylation than OsMPK3 in *CR-Osmkp1* plants (Fig. 4, G and H)

(*49*). These results suggest that OsMKP1 regulates resistance to *Xoo* in rice, mainly through dephosphorylating/inactivating OsMPK6.

OsMYB102 and OsMYB108 negatively regulate bacterial blight resistance

The rice genome encodes two MYB4 homologs, OsMYB102 and OsMYB108 (fig. S11, A and B), which were reported to negatively regulate lignin biosynthesis (*50*). We found that the transcript levels of *OsMYB102* and *OsMYB108* were unchanged in *CR-Osmkp1* or during *Xoo* infection (fig. S11C). Y2H and coIP assays indicated that OsMYB102 interacted with OsMPK6 (Fig. 5, A and B), suggesting that OsMYB102 might be an OsMPK6 substrate. To evaluate the function of OsMYB102 and OsMYB108 in *Xoo* resistance, we generated
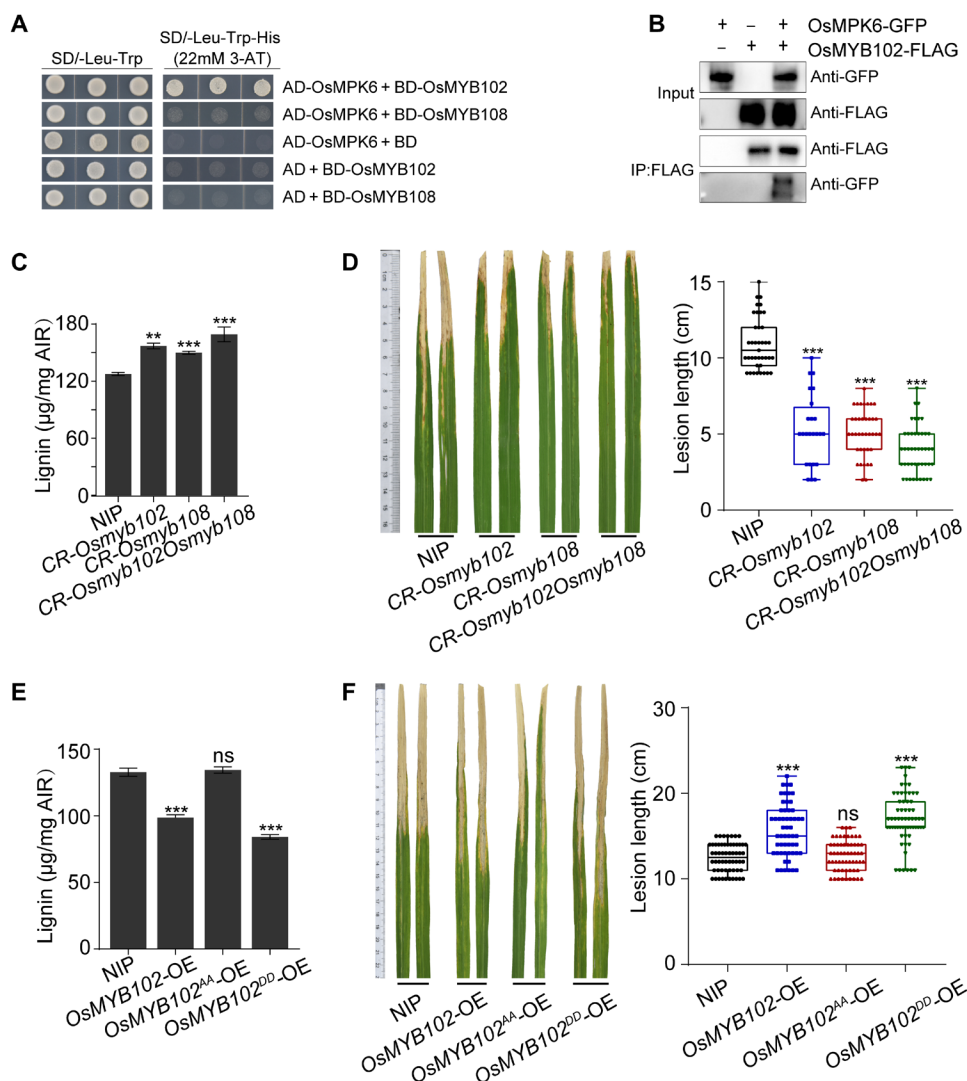
Fig. 5. OsMYB102 and OsMYB108 negatively regulate lignin biosynthesis and resistance to *Xoo*. (**A**) OsMPK6 interacts with OsMYB102 in a Y2H assay. (**B**) coIP assay of the OsMPK6-OsMYB102 interaction in *N. benthamiana*. Fusion proteins were purified and immunodetected using anti-GFP or anti-FLAG antibody. (**C**) Lignin quantification in leaves of NIP, *CR-Osmyb102*, *CR-Osmyb108*, and *CR-Osmyb102Osmyb108*, indicating that OsMYB102 and OsMYB108 negatively regulate lignin production. (**D**) Disease resistance of representative lines (left) and lesion lengths (right) of 2-month-old NIP, *CR-Osmyb102*, *CR-Osmyb108*, and *CR-Osmyb102Osmyb108* at 14 dpi with PXO99A. (**E** and **F**) Phosphorylation of OsMYB102 negatively regulates lignin biosynthesis and *Xoo* resistance. Lesions and bacterial growth of wild-type NIP, *OsMYB102*-OE, *OsMYB102^{AA}*-OE, and *OsMYB102^{DD}*-OE inoculated with PXO99A at 14 dpi. Data were shown as means ± SD; n = 3 (C and E) and n > 20 (D and F). Asterisks represented statistical significance (**P < 0.01 and ***P < 0.001, Student's t test). Experiments were repeated three times with similar results.

single knockout mutants *CR-Osmyb102* and *CR-Osmyb108* and *CR-Osmyb102Osmyb108* double mutant (fig. S11D). These mutants accumulated higher levels of lignin than wild-type NIP plants (Fig. 5C) and exhibited significantly increased resistance to *Xoo*, with *CR-Osmyb102 Osmyb108* showing stronger resistance (Fig. 5D). Thus, OsMYB102 and OsMYB108 function redundantly in the negative regulation of lignin biosynthesis and *Xoo* resistance in rice.

We further generated *OsMYB102*-OE, *OsMYB102^{AA}*-OE (Ser[4]/Ser[169] mutated to Ala), and *OsMYB102^{DD}*-OE (Ser[4]/Ser[169] mutated to Asp) transgenic plants (fig. S11E). Similar to our data in *Arabidopsis*, *OsMYB102*-OE and *OsMYB102^{DD}*-OE accumulated significantly less lignin (Fig. 5E) and were more susceptible to *Xoo* compared to the wild-type NIP control (Fig. 5F). Thus, we conclude that the MKP1-MPK3/6-MYB cascade plays a conserved role in lignin-based vascular defense in *Arabidopsis* and rice.

DISCUSSION

How plants perceive diverse pathogen signals and activate tissue-specific immune responses is an open question. One mechanism could be tissue-specific regulation of defense gene expression and metabolic pathways tailored to specific pathogen lifestyles (e.g., leaf mesophyll versus vascular infections). In this study, we uncover a protein phosphorylation–mediated mechanism that promotes vascular-specific immune: promotion of lignin biosynthesis in vascular tissues by the MKP1-MPK3/6-MYB signaling cascade (Fig. 6). This immune mechanism underlies both NHR against nonadapted vascular pathogens and host resistance to adapted vascular pathogens and is conserved in monocot rice and the dicot *Arabidopsis*.

The MAPK pathways have been to function in many signaling processes regulating plant development, abiotic stress responses, and immunity (*51–53*). The MKP1-MAPK cascade has been previously shown to negatively regulate plant resistance against mesophyll pathogens, likely through inhibiting the SA and ROS signaling pathways.

In contrast, we find that the MKP1-MAPK cascade positively regulates vascular defense through activating lignin biosynthesis via direct targeting of MYB4 transcription factors. Therefore, our study has provided an example in which the same signaling cascade leads to divergent immune outcomes against pathogens with different lifestyles, shedding light on tissue-specific defense responses in monocot and dicot plants. MPK3 and OsMPK6 are activated by *Xoo* in *mkp1* and *Osmkp1* mutant plants, respectively. Therefore, monocot and dicot plants likely adopt different MAPK targets to fine-tune a conserved defense against vascular pathogens.
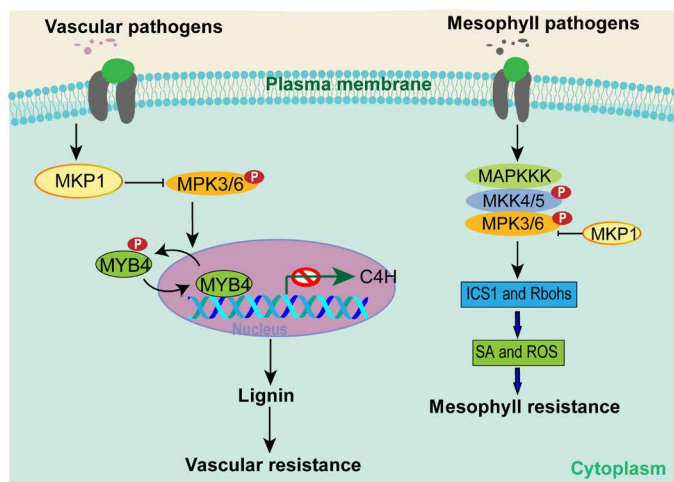
The xylem, which is developed from procambium and cambium and is composed of four types of cells—tracheids, vessels, xylem fibers, and xylem parenchyma—forms specialized vascular bundles together with the phloem and the cambium, providing structural integrity to plants and transporting water and nutrients from the soil to leaves and stems (*27, 54*). In particular, lignin is the second most abundant polymer next to cellulose in the cell walls of vascular tissues (*55*) and is often rapidly deposited through induction of lignin biosynthesis genes in responses to pathogen infection in plants (*28–30*). We discover that genes regulating lignin synthesis are less induced in the *mkp1* mutants when inoculated with *Xoo* and *Xoc*, resulting in reduced lignin accumulation in the developing xylem. The lignin-mediated vascular defense is also likely used by race-specific *R* genes against vascular pathogens in the rice-*Xoo* pathosystem. For example, the *Xa21*-mediated *Xoo* resistance is related to lignin accumulation (*56, 57*). Similarly, *Xa10* stimulates the accumulation of lignin-like phenolic compounds (*58*). This raises a fundamental question: How do these different resistance genes encoding diverse upstream immune regulators activate lignin-based vascular-specific immune responses upon perceiving *Xoo* bacteria in rice?

Our discovery of a conserved vascular-specific defense in monocot rice and dicot *Arabidopsis* will facilitate the identification of other key regulators of vascular defense through future suppressor screening. It would be worthy of further investigating how the plant immune machinery perceives diverse vascular pathogens and activates the MKP1-MAPK cascade to trigger lignin-based vascular defense. With this scenario, whether and how the rice *Xa* genes confer *Xoo* resistance are also open questions. Moreover, the discovery of the MKP1-MPK3/6-MYB cascade in vascular defense also opens the door to broadly investigating how diverse plants interact with vascular pathogens, including major crop pathogens, such as Candidatus Liberibacter asiaticus (CLas), *Xylella fastidiosa*, phytoplasmas, and vasculature-feeding insects (*16*). Hence, the basic findings from this study have broad implications for the future development of a new generation of crop resistance strategies against many devastating vascular pathogens and insects.

Fig. 6. A proposed model for the function of the MKP-MPK protein phosphorylation cascade in vascular defense in plants. *MKP1* is induced by vascular bacterial pathogens, such as *Xoo* and *Xcc*, which negatively regulate MPK3/6 through dephosphorylation. MPK3/6, in turn, activates the MYB4 transcription factor that negatively regulates lignin biosynthesis. This cascade orchestrates vascular-specific resistance against vascular pathogens and negatively regulates defense against mesophyll cell pathogens through inhibiting SA and ROS biosynthesis.

MATERIALS AND METHODS
Plant materials and growth conditions

Arabidopsis and rice were cultivated in a growth room and at an experiment station, respectively, as previously described (*59, 60*). All *Arabidopsis thaliana* experiments were in Col-0 background, including the mutants *mpk3* and *mpk6* (*61*). The transgenic lines *CR-mkp1*, *CR-myb4*, *pMKP1::MKP1/ntx1*, *pMYB4::GUS*, *MYB4*-OE, *MYB4^{AA}*-OE, and *MYB4^{DD}*-OE were generated in this study. The double mutants *mkp1 mpk3* and *mkp1 mpk6* were generated by crossing the *mkp1* with the *mpk3* and *mpk6* line, respectively. Rice transgenic lines were generated in a NIP background. Rice mutants and overexpression

lines including *CR-Osmkp1*, *CR-Osmkp1Osmpk3*, *CR-Osmkp1Osmpk6*, *CR-Osmyb102*, *CR-Osmyb108*, *CR-Osmyb102Osmyb108*, *OsMKP1*-OE, *OsMYB102*-OE, *OsMYB102^{AA}*-OE, and *OsMYB102^{DD}*-OE were generated in this study. Four-week-old *Arabidopsis* and 2-month-old rice plants were used for bacterial inoculation and disease assays.

Plasmid constructs and plant transformation

To make CRISPR-Cas9 knockout constructs, the target sequences of *MKP1*, *MYB4*, *OsMKP1*, *OsMPK3*, *OsMPK6*, *OsMYB102*, and *OsMYB108* were generated according to previously reported protocols (*62*, *63*). For overexpression constructs, the coding sequence (CDS) sequences were inserted into pCambia1300-MYC or pCambia1300-GFP (green fluorescent protein) for *Arabidopsis* transformation or inserted into PUN1301-FLAG for rice transformation with targets. The constructs were introduced into *Agrobacterium* strain GV3101 (for *Arabidopsis*) and EHA105 (for rice) and then transformed into different genetic backgrounds to produce more than 15 independent transgenic lines for each construct. Further selection and validation were based on PCR-based sequencing or Western blotting. All primers used for cloning are listed in table S1.

PXO99A-GUS–labeled strain

Pprt+gus cut from the vector pLAFR6 (*64*) was connected to binary vector pUFR034 (*65*). The recombination vector pUFR034-Pprt-gus was constructed and transformed to prepared PXO99A competent cells. The GUS that expressed transformants were screened and verified for pathogenicity by plant inoculation.

Pathogen inoculation and disease assay

For the *Arabidopsis* inoculation assay, *Pst* DC3000 [10^5 colony-forming units (CFU) ml^{-1}] was grown on LB medium [tryptone (10 g/liter), yeast extract (6 g/liter), KH$_2$PO4 (1.5 g/liter), NaCl (0.6 g/liter), MgSO$_4$·7H$_2$O (0.4 g/liter), and rifampicin (100 mg/liter); 28°C], PXO99A (2×10^7 CFU ml^{-1}) was grown on PSA medium [tryptone (10 g/liter), sucrose (10 g/liter), glutamate (1 g/liter), and cephalexin (15 mg/liter); pH 7.0; 28°C], and *8004-GFP* [10^7 CFU ml^{-1}] was grown on NYG medium [tryptone (5 g/liter), yeast extract (3 g/liter), and glycerol (20 g/liter); 28°C]. The inoculates were used for syringe infiltration. To quantify bacterial infection, *Arabidopsis* leaves were surface-sterilized using 75% ethanol, and CFUs were counted in leaf disks by serial dilutions. One technical replicate consists of four-leaf disks, and three technical replicates were included in each biological experiment. Experiments were repeated three to five times with biologically independent samples.

For rice inoculation assay, *Xoo* strain PXO99A [optical density at 600 nm (OD$_{600}$), 1.0] and *Xoc* strain RS85 (OD$_{600}$, 0.5) grown on NB medium [tryptone (10 g/liter), yeast extract (5 g/liter), and sucrose (10 g/liter); 28°C] were prepared for inoculation. Two-month-old plants were inoculated by leaf-clipping method and syringe infiltration method. Lesion length was recorded at day 14 post inoculation (dpi). To generate growth curves, 10 ml of sterile water resuspended 5 cm of leaf tissues to count CFUs (*66*, *67*). All rice inoculation experiments were repeated for three biological replicates.

RNA analysis and RNA sequencing

Total RNA was extracted using TRIzol reagent and reverse-transcribed into cDNA using ReverTra Ace qPCR RT Master Mix with genomic DNA remover. For quantitative real-time PCR analysis, TB Green Premix Ex Taq and gene-specific primers were used (table S1).

Experiments were repeated at least three times with biologically independent samples. For sample preparation, leaves of 4-week-old seedlings (Col-0 and *mkp1*) after PXO99A incubation for 12 hours was for RNA sequencing (RNA-seq), with three biological replicates for each treatment. RNA-seq analysis was performed in Shanghai Biotechnology Corporation. The entire RNA-seq dataset was deposited in the National Center for Biotechnology Information Gene Expression Omnibus under accession number GSE161152.

Y2H assay

The CDSs of the target genes were cloned into pDEST22/32 (Invitrogen) or PGADT7/PGBKT7 (Clontech). Clones were cotransformed into yeast strain AH109, grown on dropout medium (without either Trp and Leu or Trp, Leu, and His) containing 3-aminotriazole (Sigma-Aldrich, A8056). The experiments were repeated three times independently to confirm the interactions.

SLC assay

The CDSs of the genes were cloned into pCAMBIA-35S-nLuc and pCAMBIA-35S-cLuc. The clones were transformed into *Agrobacterium* strain GV3101, and bacteria solution was collected and resuspended in infiltration buffer [10 mM MgCl$_2$, 10 mM MES, and 150 mM acetosyringone (pH 5.6)] mixed with p19, incubated for 2 to 3 hours at 30°C before being infiltrated into *Nicotiana benthamiana* as previously described (*59*, *60*). Two days later, LUC signals were measured using the Luciferase Assay System (Promega) and imaged using the Tanon-5200 Chemiluminescent Imaging System. The experiments were repeated three times independently to confirm the in planta interactions.

Protein pull-down assay

Fusion proteins were expressed in *Escherichia coli*, and 30 mg of protein was bound to beads in buffer [20 mM tris-HCl (pH 7.4), 1 mM EDTA, 200 mM NaCl, 1 mM phenylmethylsulfonyl fluoride (PMSF), and 1 mM dithiothreitol (DTT)] at 4°C for 2 hours and then washed five times with the washing buffer [50 mM tris-HCl (pH 7.5), 100 mM NaCl, 10% glycerol, and 0.1% Triton X-100] to remove nonspecifically bound proteins. The binding protein was released by heating at 95°C for 5 min in 100 µl of SDS loading buffer for immunoblot.

Coimmunoprecipitation

Samples were ground in liquid nitrogen; protein was extracted using IP buffer [50 mM tris-HCl (pH 7.5), 150 mM NaCl, 1 mM EDTA, 10% glycerol, 1% Triton X-100, 1 mM PMSF, and 1× protease inhibitor cocktail (11836153001, Sigma-Aldrich)] and then vortexed and centrifuged at 12,000*g* for 10 min at 4°C. Supernatant was incubated with beads for 2 hours at 4°C, and the beads were washed four times with washing buffer [50 mM tris-HCl (pH 7.5), 150 mM NaCl, 1 mM EDTA, 10% glycerol, 1 mM PMSF, and 1× protease inhibitor cocktail]. The binding protein was released by heating at 95°C for 5 min in 100 µl of SDS loading buffer for Western blot. Proteins were resolved on a 4 to 20% Biofuraw Precast Gel (Tanon) by electrophoresis and transferred to polyvinylidene difluoride membranes using Trans-Blot Turbo blotting system (Bio-Rad). The following antibodies were used: anti-MYC (Merck Millipore, 05-724), anti-FLAG (Sigma-Aldrich, F1804), anti-GFP (Abcam, ab290), and anti-ACTIN (CMCTAG, AT0004). Immunodetection was imaged using Tanon-5200 Chemiluminescent Imaging System (Tanon), and ACTIN was used as a loading control.

MAPK activity assay

Proteins were extracted in MAPK extraction buffer [50 mM HEPES (pH 7.5), 75 mM NaCl, 5 mM EDTA, 5 mM EGTA, 50 mM β-glycerophosphate, 2 mM DTT, 0.5% Triton X-100, 1× protease inhibitor cocktail, and 1× phosphatase inhibitor cocktail (4906845001, Sigma-Aldrich)]. MAPK activities were detected using Phospho-p44/42 MAPK antibody (1:2000; 9101, Cell Signaling Technology), anti-MPK3 (1:2000; M8318, Sigma-Aldrich), and anti-MPK6 (1:2000; A7104, Sigma-Aldrich).

In vitro protein phosphorylation assay

The purified fusion proteins MKK4^{DD}-MBP (50 ng), MKK5^{DD}-MBP (50 ng), MPK3-MBP (200 ng), and MYB4-His (200 ng) produced in *E. coli* were used for in vitro protein phosphorylation assay. The proteins were incubated in reaction buffer [25 mM tris-HCl (pH 7.5), 10 mM MgCl$_2$, 1 mM DTT, and 10 mM adenosine triphosphate] at 30°C for 30 min, and the reaction was stopped by heating at 95°C for 5 min with SDS loading buffer. MYB4-His phosphorylation was visualized by immunoblotting with 10% Phos-tag Gel (Wako) as described (*68*).

GUS reporter assay

The ~2-kb promoter regions of MKP1 and MYB4 were inserted into vector 1300-GUS-Nos and then introduced into *Agrobacterium* strain GV3101 to develop GUS reporter transgenic plants. For GUS staining, plant tissues were stained in buffer [50 mM NaPO$_4$ (pH 7.0), 5 mM K$_3$Fe (CN)$_6$, 5 mM K$_4$Fe (CN)$_6$, 0.1% Triton X-100, and 1 mM X-Gluc] overnight at 37°C and then dehydrated through a graded ethanol series.

Lignin staining

For lignin staining, plant materials were soaked in FAA (50% ethanol, 5% glacial acetic acid, and 10% formaldehyde) at 4°C and then dehydrated with a graded ethanol series (100, 75, 50, and 25%) for 30 min each. Samples were fixed in resin and cut into slices (6 to 7 µm), which were then stained with 1% phloroglucinol dissolved in 12% HCl for 5 min at room temperature and observed under an optical microscope (Leica EZ4 E) as previously described (*69*).

Microscopic analysis of lignin

For histochemical observation of the cell wall autofluorescence, leaf tissues were fixed in FAA for 24 hours and then dehydrated in a graded series of ethanol from 50 to 100%. Samples were then cleared with xylene and embedded in paraffin to prepare sections (5 to 10 µm). The sections were observed under a fluorescence microscope (Zeiss LSM 880) at 488/530 nm excitation and emission (*70*).

Lignin measurement

Lignin was quantified as previously described (*71*, *72*). Briefly, leaf samples (~100 mg) were frozen and ground to powder in liquid nitrogen and washed with 70% ethanol, chloroform/methanol (1:1 v/v), and acetone. Powder samples were then evaporated until dry at 35°C, suspended in 0.1 M sodium acetate buffer (pH 5.0), and heated for 20 min at 80°C. After adding 35 µl of amylase [H$_2$O (50 µg/ml); from *Bacillus* species; Sigma-Aldrich] and 17 µl of pullulanase (17.8 U from *Bacillus acidopullulyticus*; Sigma-Aldrich), samples were incubated overnight at 37°C and digested with 100 µl of 25% acetyl bromide in acetic acid at 50°C for 2 hours. The samples were mixed with 2 M NaOH (400 µl), 0.5 M hydroxylamine hydrochloride

(70 µl), and acetic acid to 2 ml. Absorbance was measured at 280 nm. The content of acetyl bromide soluble lignin (%ABSL) was calculated using Beer's law with extinction coefficient of 15.69 mg/cm per liter for *Arabidopsis* and 17.2 mg/cm per liter for rice.

SA analysis

For total and free SA measurement (*12*), leaf tissues (100 mg) were ground in liquid nitrogen and extracted with 90% methanol, and 250 ng of *o*-anisic acid was used as an internal standard. The samples were subjected to phase separation in ethyl acetate/cyclopentane (1:1 v/v) and then evaporated and solubilized in 20% methanol with 5% trichloroacetic acid. Filtered extracts were quantified using high-performance liquid chromatography, and fluorescence was recorded with excitation/emission wavelengths of 305/407 nm for *o*-anisic acid and SA.

Microscopic observation of bacteria in planta

For scanning electron micrograph (SEM) of bacteria, plant materials inoculated with pathogens were soaked in FAA at 4°C; dehydrated with 50, 70, 85, and 100% ethanol for 5 min each; dried with CO$_2$ critical point drier; and observed under Zeiss Merlin Compact SEM. For TEM of bacteria, plant materials inoculated with pathogens were soaked in 2.5% glutaraldehyde solution at 4°C and embedded with conventional methods, and slices were observed with Hitachi H-7650 TEM.

Statistical analysis

In this study, all values are presented as means ± SD, and the number (*n*) of samples or replicates are indicated in the figure legends. Significant differences were analyzed using Student's *t* test for pairwise comparisons and one-way or two-way analysis of variance (ANOVA) with Tukey's test between multiple groups comparison indicated with *P* values or different letters.

SUPPLEMENTARY MATERIALS

Supplementary material for this article is available at https://science.org/doi/10.1126/sciadv.abg8723

View/request a protocol for this paper from *Bio-protocol*.

REFERENCES AND NOTES

1. W. J. Lucas, A. Groover, R. Lichtenberger, K. Furuta, S. R. Yadav, Y. Helariutta, X. Q. He, H. Fukuda, J. Kang, S. M. Brady, J. W. Patrick, J. Sperry, A. Yoshida, A. F. López-Millán, M. A. Grusak, P. Kachroo, The plant vascular system: Evolution, development and functions. *J. Integr. Plant Biol.* **55**, 294–388 (2013).
2. D. O. Niño-Liu, P. C. Ronald, A. J. Bogdanove, *Xanthomonas oryzae* pathovars: Model pathogens of a model crop. *Mol. Plant Pathol.* **7**, 303–324 (2006).
3. A. Guo, J. E. Leach, Examination of rice hydathode water pores exposed to *Xanthomonas campestris* pv. *oryzae*. *Phytopathology* **79**, 433–436 (1989).
4. J. G. Vicente, E. B. Holub, *Xanthomonas campestris* pv. *campestris* (cause of black rot of crucifers) in the genomic era is still a worldwide threat to brassica crops. *Mol. Plant Pathol.* **14**, 2–18 (2013).
5. T. M. Lowe, F. Ailloud, C. Allen, Hydroxycinnamic acid degradation, a broadly conserved trait, protects *Ralstonia solanacearum* from chemical plant defenses and contributes to root colonization and virulence. *Mol. Plant Microbe Interact.* **28**, 286–297 (2015).
6. N. Denancé, P. Ranocha, N. Oria, X. Barlet, M.-P. Rivière, K. A. Yadeta, L. Hoffmann, F. Perreau, G. Clément, A. Maia-Grondard, G. C. M. van den Berg, B. Savelli, S. Fournier, Y. Aubert, S. Pelletier, B. P. H. J. Thomma, A. Molina, L. Jouanin, Y. Marco, D. Goffner, Arabidopsis *wat1* (*walls are thin1*)-mediated resistance to the bacterial vascular pathogen, *Ralstonia solanacearum*, is accompanied by cross-regulation of salicylic acid and tryptophan metabolism. *Plant J.* **73**, 225–239 (2013).
7. E. F. Fradin, B. P. H. J. Thomma, Physiology and molecular aspects of *Verticillium* wilt diseases caused by *V. dahliae* and *V. albo-atrum*. *Mol. Plant Pathol.* **7**, 71, –86 (2006).

8. N. Montes-Osuna, J. Mercado-Blanco, *Verticillium* wilt of olive and its control: What did we learn during the last decade? *Plants* **9**, 753 (2020).

9. S. Genin, T. P. Denny, Pathogenomics of the *Ralstonia solanacearum* species complex. *Annu. Rev. Phytopathol.* **50**, 67–89 (2012).

10. M. Gao, Y. He, X. Yin, X. Zhong, B. Yan, B. Wu, J. Chen, X. Li, K. Zhai, Y. Huang, X. Gong, H. Chang, S. Xie, J. Liu, J. Yue, J. Xu, G. Zhang, Y. Deng, E. Wang, D. Tharreau, G. Wang, W. Yang, Z. He, Ca²⁺ sensor-mediated ROS scavenging suppresses rice immunity and is exploited by a fungal effector. *Cell* **184**, 5391–5404.e17 (2021).

11. Q. You, K. Zhai, D. Yang, W. Yang, J. Wu, J. Liu, W. Pan, J. Wang, X. Zhu, Y. Jian, J. Liu, Y. Zhang, Y. Deng, Q. Li, Y. Lou, Q. Xie, Z. He, An E3 ubiquitin ligase-bag protein module controls plant innate immunity and broad-spectrum disease resistance. *Cell Host Microbe* **20**, 758–769 (2016).

12. X. Yin, B. Zou, X. Hong, M. Gao, W. Yang, X. Zhong, Y. He, P. Kuai, Y. Lou, J. Huang, J. Hua, Z. He, Rice copine genes *OsBON1* and *OsBON3* function as suppressors of broad-spectrum disease resistance. *Plant Biotechnol. J.* **16**, 1476–1487 (2018).

13. J. M. Zhou, Y. Zhang, Plant immunity: Danger perception and signaling. *Cell* **181**, 978–989 (2020).

14. J. D. Jones, R. E. Vance, J. L. Dangl, Intracellular innate immune surveillance devices in plants and animals. *Science* **354**, aaf6395 (2016).

15. X. F. Xin, B. Kvitko, S. Y. He, *Pseudomonas syringae*: What it takes to be a pathogen. *Nat. Rev. Microbiol.* **16**, 316–328 (2018).

16. Y. Jiang, C. X. Zhang, R. Chen, S. Y. He, Challenging battles of plants with phloem-feeding insects and prokaryotic pathogens. *Proc. Natl. Acad. Sci. U.S.A.* **116**, 23390–23397 (2019).

17. S. Chatterjee, R. P. Almeida, S. Lindow, Living in two worlds: The plant and insect lifestyles of *Xylella fastidiosa*. *Annu. Rev. Phytopathol.* **46**, 243–271 (2008).

18. M. A. Jacques, M. Arlat, A. Boulanger, T. Boureau, S. Carrère, S. Cesbron, N. W. Chen, S. Cociancich, A. Darrasse, N. Denancé, M. Fischer-Le Saux, L. Gagnevin, R. Koebnik, E. Lauber, L. D. Noël, I. Pieretti, P. Portier, O. Pruvost, A. Rieux, I. Robène, M. Royer, B. Szurek, V. Verdier, C. Vernière, Using ecology, physiology, and genomics to understand host specificity in *Xanthomonas*. *Annu. Rev. Phytopathol.* **54**, 163–187 (2016).

19. A. Cerutti, A. Jauneau, E. Auriac Lauber, Y. Martinez, S. Chiarenza, N. Leonhardt, R. Berthomé, L. D. Noël, Immunity at cauliflower hydathodes controls systemic infection by *Xanthomonas campestris* pv *campestris*. *Plant Physiol.* **174**, 700–716 (2017).

20. V. Verdier, L. R. Triplett, A. W. Hummel, R. Corral, R. A. Cernadas, C. L. Schmidt, A. J. Bogdanove, J. E. Leach, Transcription activator-like (TAL) effectors targeting *OsSWEET* genes enhance virulence on diverse rice (*Oryza sativa*) varieties when expressed individually in a TAL effector-deficient strain of *Xanthomonas oryzae*. *New Phytol.* **196**, 1197–1207 (2012).

21. J. H. Zhou, Z. Peng, J. Y. Long, D. Sosso, B. Liu, J. S. Eom, S. Huang, S. Z. Liu, C. Vera Cruz, W. B. Frommer, F. F. White, B. Yang, Gene targeting by the TAL effector PthXo2 reveals cryptic resistance gene for bacterial blight of rice. *Plant J.* **82**, 632–643 (2015).

22. G. Jha, R. Rajeshwari, R. V. Sonti, Functional interplay between two *Xanthomonas oryzae* pv. *oryzae* secretion systems in modulating virulence on rice. *Mol. Plant Microbe Interact.* **20**, 31–40 (2007).

23. L. Tayi, R. Maku, H. K. Patel, R. V. Sonti, Action of multiple cell wall-degrading enzymes is required for elicitation of innate immune responses during *Xanthomonas oryzae* pv. *oryzae* infection in rice. *Mol. Plant Microbe Interact.* **29**, 599–608 (2016).

24. L. Tayi, S. Kumar, R. Nathawat, A. S. Haque, R. V. Maku, H. K. Patel, R. Sankaranarayanan, R. V. Sonti, A mutation in an exoglucanase of *Xanthomonas oryzae* pv. *oryzae*, which confers an endo mode of activity, affects bacterial virulence, but not the induction of immune responses, in rice. *Mol. Plant Pathol.* **19**, 1364–1376 (2018).

25. E. Gluck-Thaler, A. Cerutti, A. L. Perez-Quintero, J. Butchacas, V. Roman-Reyna, V. N. Madhavan, D. Shantharaj, M. V. Merfa, C. Pesce, A. Jauneau, T. Vancheva, J. M. Lang, C. Allen, V. Verdier, L. Gagnevin, B. Szurek, G. T. Beckham, L. De La Fuente, H. K. Patel, R. V. Sonti, C. Bragard, J. E. Leach, L. D. Noël, J. C. Slot, R. Koebnik, J. M. Jacobs, Repeated gain and loss of a single gene modulates the evolution of vascular plant pathogen lifestyles. *Sci. Adv.* **6**, eabc4516 (2020).

26. B. Samal, S. Chatterjee, New insight into bacterial social communication in natural host: Evidence for interplay of heterogeneous and unison quorum response. *PLOS Genet.* **15**, e1008395 (2019).

27. K. Růžička, R. Ursache, J. Hejátko, Y. Helariutta, Xylem development—From the cradle to the grave. *New Phytol.* **207**, 519–535 (2015).

28. S. Lee, Y. Sharm, T. K. Lee, M. Chang, K. R. Davis, Lignification induced by *Pseudomonads* harboring avirulent genes on *Arabidopsis*. *Mol. Cells* **12**, 25–31 (2001).

29. F. G. Malinovsky, J. U. Fangel, W. G. T. Willats, The role of the cell wall in plant immunity. *Front. Plant Sci.* **5**, 178 (2014).

30. J. Yoon, H. Choi, G. An, Roles of lignin biosynthesis and regulatory genes in plant development. *J. Integr. Plant Biol.* **57**, 902–912 (2015).

31. J. Zhou, C. Lee, R. Zhong, Z. H. Ye, MYB58 and MYB63 are transcriptional activators of the lignin biosynthetic pathway during secondary cell wall formation in *Arabidopsis*. *Plant Cell* **21**, 248–266 (2009).

32. E. Li, A. Bhargava, W. Qiang, M. C. Friedmann, N. Forneris, R. A. Savidge, L. A. Johnson, S. D. Mansfield, B. E. Ellis, C. J. Douglas, The class II *KNOX* gene *KNAT7* negatively regulates secondary wall formation in *Arabidopsis* and is functionally conserved in *Populus*. *New Phytol.* **194**, 102–115 (2012).

33. H. Jin, E. Cominelli, P. Bailey, A. Parr, F. Mehrtens, J. Jones, C. Tonelli, B. Weisshaar, C. Martin, Transcriptional repression by AtMYB4 controls production of UV-protecting sunscreens in *Arabidopsis*. *EMBO J.* **19**, 6150–6161 (2000).

34. M. R. Hemm, K. M. Herrmann, C. Chapple, AtMYB4: A transcription factor general in the battle against UV. *Trend. Plant Sci.* **6**, 135–136 (2001).

35. M. Mitra, P. Agarwal, A. Kundu, V. Banerjee, S. Roy, Investigation of the effect of UV-B light on *Arabidopsis* MYB4 (AtMYB4) transcription factor stability and detection of a putative MYB4-binding motif in the promoter proximal region of AtMYB4. *PLOS ONE* **14**, e0220123 (2019).

36. G. Ye, N. Hong, L. F. Zou, H. S. Zou, M. Zakria, G. P. Wang, G. Y. Chen, Tale-based genetic diversity of chinese isolates of the citrus canker pathogen *Xanthomonas citri* subsp *citri*. *Plant Dis.* **97**, 1187–1194 (2013).

37. Z. Li, L. F. Zou, G. Ye, L. Xiong, Z. Y. Ji, M. Zakria, N. Hong, G. P. Wang, G. Y. Chen, A potential disease susceptibility gene *CsLOB* of citrus is targeted by a major virulence effector PthA of *Xanthomonas citri* subsp *citri*. *Mol. Plant* **7**, 912–915 (2014).

38. V. Bartetzko, S. Sonnewald, F. Vogel, K. Hartner, R. Stadler, U. Z. Hammes, F. Börnke, The *Xanthomonas campestris* pv. *vesicatoria* type III effector protein XopJ inhibits protein secretion: Evidence for interference with cell wall-associated defense responses. *Mol. Plant Microbe Interact.* **22**, 655–664 (2009).

39. J. P. R. Priller, S. Reid, P. Konein, P. Dietrich, S. Sonnewald, The *Xanthomonas campestris* pv. *vesicatoria* type-3 effector XopB inhibits plant defence responses by interfering with ROS production. *PLOS ONE* **11**, e0159107 (2016).

40. C. F. An, Z. L. Mou, Non-host defense response in a novel *Arabidopsis-Xanthomonas citri* subsp *citri* pathosystem. *PLOS ONE* **7**, e31130 (2012).

41. S. Bartels, J. C. Anderson, M. A. González Besteiro, A. Carreri, H. Hirt, A. Buchala, J. P. Métraux, S. C. Peck, R. Ulm, MAP kinase phosphatase1 and protein tyrosine phosphatase1 are repressors of salicylic acid synthesis and SNC1-mediated responses in *Arabidopsis*. *Plant Cell* **21**, 2884–2897 (2009).

42. T. Asai, G. Tena, J. Plotnikova, M. R. Willmann, W. L. Chiu, L. Gomez-Gomez, T. Boller, F. M. Ausubel, J. Sheen, MAP kinase signalling cascade in *Arabidopsis* innate immunity. *Nature* **415**, 977–983 (2002).

43. R. Ulm, K. Ichimura, T. Mizoguchi, S. C. Peck, T. Zhu, X. Wang, K. Shinozaki, J. Paszkowski, Distinct regulation of salinity and genotoxic stress responses by *Arabidopsis* MAP kinase phosphatase 1. *EMBO J.* **21**, 6483–6493 (2002).

44. Z. Q. Fu, X. Dong, Systemic acquired resistance: Turning local infection into global defense. *Annu. Rev. Plant Biol.* **64**, 839–863 (2013).

45. K. Tsuda, M. Sato, J. Glazebrook, J. D. Cohen, F. Katagiri, Interplay between MAMP-triggered and SA-mediated defense responses. *Plant J.* **53**, 763–775 (2008).

46. D. Ren, H. Yang, S. Zhang, Cell death mediated by MAPK is associated with hydrogen peroxide production in *Arabidopsis*. *J. Biol.Chem.* **277**, 559–565 (2002).

47. A. Pitzschke, Modes of MAPK substrate recognition and control. *Trends Plant Sci.* **20**, 49–55 (2015).

48. S. Katou, K. Kuroda, S. Seo, Y. Yanagawa, T. Tsuge, M. Yamazaki, A. Miyao, H. Hirochika, Y. Ohashi, A calmodulin-binding mitogen-activated protein kinase phosphatase is induced by wounding and regulates the activities of stress-related mitogen-activated protein kinases in rice. *Plant Cell Physiol.* **48**, 332–344 (2007).

49. L. Helft, M. Thompson, A. F. Bent, Directed evolution of FLS2 towards novel flagellin peptide recognition. *PLOS ONE* **11**, e0157155 (2016).

50. T. Miyamoto, R. Takada, Y. Tobimatsu, Y. Takeda, S. Suzuki, M. Yamamura, K. Osakabe, Y. Osakabe, M. Sakamoto, T. Umezawa, OsMYB108 loss-of-function enriches p-coumaroylated and tricin lignin units in rice cell walls. *Plant J.* **98**, 975–987 (2019).

51. S. Bartels, M. A. González Besteiro, D. Lang, R. Ulm, Emerging functions for plant MAP kinase phosphatases. *Trends Plant Sci.* **15**, 322–329 (2010).

52. A. Shankar, N. Agrawal, M. Sharma, A. Pandey, K. P. M. Girdhar, Role of protein tyrosine phosphatases in plants. *Curr. Genomics* **16**, 224–236 (2015).

53. X. Meng, S. Zhang, MAPK cascades in plant disease resistance signaling. *Annu. Rev. Phytopathol.* **51**, 245–266 (2013).

54. K. A. Yadeta, B. P. H. J. Thomma, The xylem as battleground for plant hosts and vascular wilt pathogens. *Front. Plant Sci.* **4**, 97 (2013).

55. G. Neutelings, Lignin variability in plant cell walls: Contribution of new models. *Plant Sci.* **181**, 379–386 (2011).

56. W. Song, G. L. Wang, L. L. Chen, H. S. Kim, L. Y. Pi, T. Holsten, J. Gardner, B. Wang, W. X. Zhai, L. H. Zhu, C. Fauquet, P. Ronald, A receptor kinase-like protein encoded by the rice disease resistance gene, *Xa21*. *Science* **270**, 1804–1806 (1995).

57. Shamsunnaher, X. Chen, X. Zhang, X. Wu, X. Huang, W. Song, Rice immune sensor XA21 differentially enhances plant growth and survival under distinct levels of drought. *Sci. Rep.* **10**, 16938 (2020).

58. P. J. Reimers, J. E. Leach, Race-specific resistance to *Xanthomonas oryzae* pv *oryzae* conferred by bacterial blight resistance gene *Xa10* in rice (*Oryza Sativa*) involves accumulation of a lignin-like substance in host tissues. *Physiol. Mol. Plant Pathol.* **38**, 39–55 (1991).

59. J. Liu, L. Feng, X. Gu, X. Deng, Q. Qiu, Q. Li, Y. Zhang, M. Wang, Y. Deng, E. Wang, Y. He, I. Bäurle, J. Li, X. Cao, Z. He, An H3K27me3 demethylase-HSFA2 regulatory loop orchestrates transgenerational thermomemory in Arabidopsis. *Cell Res.* **29**, 379–390 (2019).

60. K. Zhai, Y. Deng, D. Liang, J. Tang, J. Liu, B. Yan, X. Yin, H. Lin, F. Chen, D. Yang, Z. Xie, J. Y. Liu, Q. Li, L. Zhang, Z. He, RRM transcription factors interact with NLRs and regulate broad-spectrum blast resistance in rice. *Mol. Cell* **74**, 996–1009.e7 (2019).

61. J. Xu, J. Xie, C. Yan, X. Zou, D. Ren, S. Zhang, A chemical genetic approach demonstrates that MPK3/MPK6 activation and NADPH oxidase-mediated oxidative burst are two independent signaling events in plant immunity. *Plant J.* **77**, 222–234 (2014).

62. X. Ma, Q. Zhang, Q. Zhu, W. Liu, Y. Chen, R. Qiu, B. Wang, Z. Yang, H. Li, Y. Lin, Y. Xie, R. Shen, S. Chen, Z. Wang, Y. Chen, J. Guo, L. Chen, X. Zhao, Z. Dong, Y. G. Liu, A robust CRISPR/Cas9 system for convenient, high-efficiency multiplex genome editing in monocot and dicot plants. *Mol. Plant* **8**, 1274–1284 (2015).

63. L. Yan, S. Wei, Y. Wu, R. Hu, H. Li, W. Yang, Q. Xie, High-efficiency genome editing in *Arabidopsis* using YAO promoter-driven CRISPR/Cas9 system. *Mol. Plant* **8**, 1820–1823 (2015).

64. G. T. Lu, Z. F. Ma, J. R. Hu, D. J. Tang, Y. Q. He, J. X. Feng, J. L. Tang, A novel locus involved in extracellular polysaccharide production and virulence of *Xanthomonas campestris* pathovar *campestris*. *Microbiology* **153**, 737–746 (2007).

65. R. Defeyter, C. I. Kado, D. W. Gabriel, Small, stable shuttle vectors for use in *Xanthomonas*. *Gene* **88**, 65–72 (1990).

66. P. A. Bartonwillis, P. D. Roberts, A. Guo, J. E. Leach, Growth dynamics of *Xanthomonas campestris* pv *oryzae* in leaves of rice differential cultivars. *Phytopathology* **79**, 573–578 (1989).

67. B. Yang, A. Bogdanove, Inoculation and virulence assay for bacterial blight and bacterial leaf streak of rice. *Methods Mol. Biol.* **956**, 249–255 (2013).

68. L. Jiang, J. C. Anderson, M. A. Gonzalez Besteiro, S. C. Peck, Phosphorylation of Arabidopsis MAP kinase phosphatase 1 (MKP1) is required for PAMP responses and resistance against bacteria. *Plant Physiol.* **175**, 1839–1852 (2017).

69. J. Gui, L. Luo, Y. Zhong, J. Sun, T. Umezawa, L. Li, Phosphorylation of LTF1, an MYB transcription factor in populus, acts as a sensory switch regulating lignin biosynthesis in wood cells. *Mol. Plant* **12**, 1325–1337 (2019).

70. F. Baldacci-Cresp, C. Spriet, L. Twyffels, A. S. Blervacq, G. Neutelings, M. Baucher, S. Hawkins, A rapid and quantitative safranin-based fluorescent microscopy method to evaluate cell wall lignification. *Plant J.* **102**, 1074–1089 (2020).

71. C. E. Foster, T. M. Martin, M. Pauly, Comprehensive compositional analysis of plant cell walls (lignocellulosic biomass) part I: Lignin. *J. Vis. Exp.* 1745 (2010).

72. R. de Cássia Siqueira-Soares, A. Finger-Teixeira, D. Matias, de Oliveira, A. P. Ferro, G. J. da Rocha, M. d. L. L. Ferrarese, W. Dantas, dos Santos, O. Ferrarese-Filho, The acetyl bromide method is faster, simpler and presents best recovery of lignin in different herbaceous tissues than Klason and thioglycolic acid methods. *PLOS ONE* **9**, e110000 (2014).

An MKP-MAPK protein phosphorylation cascade controls vascular immunity in plants

Hui LinMuyang WangYing ChenKinya NomuraShugang HuiJinshan GuiXiawei ZhangYue WuJiyun LiuQun LiYiwen DengLaigeng LiMeng YuanShiping WangSheng Yang HeZuhua He

View the article online
https://www.science.org/doi/10.1126/sciadv.abg8723
Permissions
https://www.science.org/help/reprints-and-permissions

Use of this article is subject to the Terms of service